OPTRONIC™
LABORATORIES

PROBING THE ARCHITECTURE OF CHAMELEON SECRETIN RECEPTORS WITH FRET USING AOTF-BASED SPECTRAL IMAGING

Reprinted with permission by Cayle S. Lisenbee, Kaleeckal g. Harikumar, Laurence J. Miller

Cancer Center and Dept. of Molecular Pharmacology and Experimental Therapeutics, Mayo ClinicJune 2009

August 2008

PROBING THE ARCHITECTURE OF CHAMELEON SECRETIN RECEPTORS WITH FRET USING AOTF-BASED SPECTRAL IMAGING[1]

Cayle S. Lisenbee, Kaleeckal G. Harikumar, Laurence J. Miller
From the Cancer Center and Department of Molecular Pharmacology and Experimental Therapeutics, Mayo Clinic, Scottsdale, Arizona, 85259

Running Title: Chameleon Receptors for Intramolecular FRET

Address correspondence to: Laurence J. Miller, Mayo Clinic, 13400 E. Shea Blvd., Scottsdale, AZ 85259. Tel: 480-301-6650; Fax: 480-301-6969; E-mail: miller@mayo.edu

The molecular structure and agonist-induced conformational changes of Family B G protein-coupled receptors are poorly understood. In this work, we have developed and characterized a series of cyan and yellow fluorescent protein (CFP/YFP[2]) "chameleons" of the prototypic secretin receptor for use in various functional and fluorescence analyses of receptor structure. CFP insertions within the first or second intracellular loops of this receptor were tolerated poorly or partially, respectively, in receptors tagged with a carboxyl-terminal YFP that itself had no effect on secretin binding or cAMP production. Similar CFP insertions within the third intracellular loop resulted in plasma membrane-localized receptors that bound secretin and signaled normally. Fluorescence resonance energy transfer (FRET) signals recorded with an acousto-optic tunable filter microscope placed the carboxyl-terminal YFP closest to the first loop CFP and farthest from the second loop CFP. Third loop chameleons localized to the plasma membrane exhibited a significant decrease in FRET upon secretin agonist, but not PG97-269 antagonist, treatments of cells stably expressing these fully functional receptors. These data reveal changes in the relative positions of intracellular structures that help support a model for secretin receptor activation and establish spectral imaging as a useful tool for energy transfer studies.

G protein-coupled receptors (GPCRs) are heptahelical, integral plasma membrane proteins that are activated by a diverse set of pharmacologically important molecules to initiate intracellular signaling cascades. Several members of this superfamily have become important targets for therapeutic intervention in disease. Drugs that act at these receptors target their natural ligand-binding sites, as well as other recognized sites for allosteric drug action. While current approaches to drug discovery have been successful, much remains to be learned of the precise conformational changes and intracellular rearrangements that occur upon receptor activation. It is hoped that such an understanding might open new pathways for the development and refinement of receptor-active drugs.

Data from spin labeling, chemical crosslinking, and receptor mutagenesis approaches have led to a proposal for a common molecular mechanism of GPCR activation (1,2). Best understood for rhodopsin and other Family A receptors, this mechanism involves the communication of ligand-induced conformational information across the transmembrane (TM) core for the activation of G protein-mediated guanine nucleotide exchange at the intracellular face of the molecule. In rhodopsin, this communication process includes documented shifts in the relative positions of certain membrane-spanning helices (3). Some of these same movements have been inferred for Family B receptors, such as the shift in the relative positions of helices 3 and 6 in the parathyroid hormone receptor (4). However, structural differences between Family A and B receptors suggest that these rearrangements may not be extrapolated to all heptahelical GPCRs, in particular because the helical bundle of Family B receptors probably assumes a structure that differs significantly from that of Family A receptors (5).

Recently, we have shown that secretin receptor (SecR), and perhaps all Family B GPCRs, may utilize a novel activation mechanism that distinguishes it from the more extensively studied rhodopsin-like receptors (6). Several members of this small subset of GPCRs, including the glucagon-like peptide and parathyroid hormone

receptors, have garnered much interest as drug targets for the treatment of diabetes and bone disorders. Secretin receptor is a prototypic member of this family that stimulates pancreaticobiliary ductular bicarbonate secretion upon binding a 27-residue secretin peptide agonist (7). Ligand binding studies have demonstrated spatial approximations of secretin agonist analogs with the receptor amino-terminal domain (8-13) and with the top of the sixth TM helix (14,15). The amino terminus is thought to provide a docking platform for natural peptide ligands that changes conformation upon agonist binding to expose an endogenous, agonist ligand that can interact with the receptor core (16). Comprised of as little as three residues within a short loop sequence of the receptor's amino-terminal domain, this secondary ligand acts with full agonist potency through the top of the sixth TM helix, where it is presumed to induce changes in the helical bundle that then stimulate signaling through G_s-mediated activation of adenylate cyclase (16). However, the precise means by which these changes are propagated to the intracellular face of the receptor for G protein coupling, stimulation, and turnover are poorly understood.

Current understanding of the activation of Family B GPCRs has come from photoaffinity labeling and biophysical studies performed with secretin analogs containing photolabile or fluorescent residues (8-15,17-19). Because these interactions have provided snapshots of receptor structure only from the perspective of the extracellular environment, our goal in the present work was to develop new tools that would allow for real-time monitoring of the receptor's intracellular architecture in living cells. Therefore, we constructed and characterized a series of dual reporter-tagged secretin receptor variants, or "chameleons", in which enhanced cyan and yellow fluorescent protein (CFP and YFP) tags were incorporated strategically within functionally-relevant intracellular loop and carboxyl-terminal domains of secretin receptor. Integration of these tags effectively placed positional markers for two different receptor domains within the same receptor molecule, where it was predicted that conformational rearrangements could be detected as changes in fluorescence resonance energy transfer (FRET) between the strategically positioned fluorescent reporters. This approach was introduced recently in a kinetic study of parathyroid hormone receptor activation (20), but that work employed a limited number of chameleon receptor variants for which the energy transfer changes at best represented only 20% of the total signal.

We attempted to expand the scope of that previous study by incorporating CFP systematically into each of secretin receptor's three intracellular loops. These mutants comprised a unique set of receptors that included fully functional variants, as well as those in which biological activity was uncoupled from high affinity binding. In its first application, an acousto-optic tunable filter system was used in conjunction with standard epifluorescence microscopy for the collection of wavelength-registered serial fluorescence emission micrographs. Emission intensities from these images were compiled into pixel-specific spectra that through careful correction and analysis provided enhanced flexibility over fixed-bandwidth filter methods for calculating FRET ratios at the single cell level. Moreover, these FRET signals were localized to plasma membrane regions for recording observed signal changes upon ligand binding. From these findings, we were able to position secretin receptor's three intracellular loops relative to its carboxyl terminus and then formulate predictions on how the third loop and carboxyl terminus may move apart upon ligand binding. These findings are discussed in the context of our current understanding of secretin receptor function, and for how they demonstrate promising new ways to apply advanced fluorescence techniques for the study of receptor structure and activation.

EXPERIMENTAL PROCEDURES

Materials: Molecular biology reagents for receptor mutagenesis were obtained from New England Biolabs (Beverly, MA), Stratagene (La Jolla, CA), Bio-Rad Laboratories (Hercules, CA), Eppendorf (Hamburg, Germany), and Qiagen (Valencia, CA). Cell culture supplies and Lipofectamine were purchased from Invitrogen (San Diego, CA), serum supplements from HyClone Laboratories (Logan, UT), and non-

enzymatic cell dissociation solution from Sigma-Aldrich (St. Louis, MO). Formaldehyde and Vectashield were provided by Ted Pella (Redding, CA) and Vector Laboratories (Burlingame, CA), respectively. Binding and biological activity assays employed [Tyr^{10}]secretin and/or natural rat secretin peptides that were synthesized in our laboratory (21) and shown to be active at human secretin receptors expressed in intact cells (10). The Tyr^{10} residue was derivatized by oxidative radioiodination to form the ^{125}I-[Tyr^{10}]secretin radioligand as described previously (21). Reagents not listed here were of the highest grade available, as appropriate for the given experiment.

Receptor Mutagenesis: Recombinant coding sequences were expressed constitutively from the CMV promoter in the eukaryotic expression vector pcDNA3 (Invitrogen). All receptor mutations were incorporated into the plasmids pcDNA3/SecR and pcDNA3/SecR-YFP which code, respectively, for native and carboxyl-terminally tagged versions of human secretin receptor (22,23). Its predicted amino acid sequence was aligned with other closely-related receptors using the CLUSTALW algorithm, and from these alignments were determined the most highly nonconserved residues within the receptor's intracellular loop regions that would be most tolerant of fluorescent protein insertions. These regions corresponded to first loop positions 510 and 513, second loop positions 732 and 735, and the third loop position 993, where the numbers refer to the nucleotide positions within the human SecR open reading frame after which was inserted the coding sequence for an enhanced CFP (numbering begins with the first nucleotide of the start codon). The latter was amplified from pECFP-N1 (Clontech, Mountain View, CA) with primers that added an in-frame NheI site in place of the start codon and an in-frame XbaI site that replaced the stop codon. The resulting products were ligated by TA cloning into pCRII (Invitrogen) to yield pCRII/NheI-CFP-XbaI. The NheI/XbaI fragment from this plasmid was ligated into NheI-digested versions of pcDNA3/SecR and pcDNA3/SecR-YFP that had been mutated in QuikChange (Stratagene) site-directed mutagenesis reactions with primers that inserted a unique NheI site at each of the nonconserved loop positions identified previously. These reactions yielded a set of CFP donor-only control receptors, as well as the corresponding CFP/YFP dual-tagged chameleon variants (Table 1). All DNA sequences were confirmed by both restriction digestion and automated dye-terminator cycle sequencing.

Cell Cultures and Transfections: African green monkey kidney (COS) cells were propagated in Dulbecco's modified Eagle's growth medium (DMEM) and transfected in diethylaminoethyl (DEAE)-dextran solutions as described previously (24). Transfected cells were lifted with trypsin, transferred to coverslips or 24-well plates as appropriate, and then incubated for an additional 24 to 48 h to allow transient gene expression. All transfections received a constant 3 μg of plasmid DNA per 10-cm Petri dish regardless of the downstream application. Chinese hamster ovary (CHO) cells obtained from the American Type Culture Collection (Manassas, VA) were grown in a Ham's F-12 nutrient mixture containing 5% (v/v) Fetal Clone II serum. The cells were passaged twice per week on Corning (Acton, MA) tissue culture flasks and maintained in a humidified atmosphere of 5% (v/v) CO_2 at 37 °C. Stable transfections were accomplished with Lipofectamine and PLUS reagents according to the manufacturer's instructions. The transfected, G418-resistant cells then were subjected to our standard limiting dilution procedure, followed by screening of the resulting clonal lines in secretin binding and/or fluorescence assays (see below). Those clones exhibiting binding and fluorescence attributes most like YFP-tagged wild type receptors were characterized further as stably expressing chameleon cell lines.

Confocal Microscopy: Subcellular localizations of the YFP-tagged receptor variants from each group of chameleon constructs were evaluated in transfected COS cells seeded to 25 mm coverslips in 6-well plates. The adherent cells were fixed immediately after removal from the growth incubator in freshly-diluted 2% (w/v) formaldehyde in phosphate-buffered saline (PBS) for 15 min at room temperature. The fixed cells were washed in three 5-min exchanges of PBS, pH 7.4, and then mounted on microscope slides in Vectashield to prevent photobleaching. Receptors were localized within cells as described previously (22) using a Zeiss (Thornwood, NY) LSM 510 confocal microscope that was configured

specifically for capturing YFP emissions. Digital images were background-subtracted, adjusted for contrast where necessary, and then assembled into figures using Adobe Photoshop 7.0 (Mountain View, CA).

Receptor Binding Assays: Transfected cells in 24-well plates were tested for the ability of expressed SecR variants to bind secretin agonists saturably and with high affinity (22). Cells were washed twice in Krebs-Ringers-HEPES (KRH) solution (25 mM HEPES, pH 7.4, 104 mM NaCl, 5 mM KCl, 1 mM KH_2PO_4, 1.2 mM $MgSO_4$, 2 mM $CaCl_2$) containing 0.2% (w/v) bovine serum albumin and 0.01% (w/v) soybean trypsin inhibitor, and then were treated with increasing amounts of unlabeled secretin (from 0 to 1 μM) for 1 h at room temperature in the presence of constant amounts of radiolabeled ^{125}I-[Tyr^{10}]secretin (roughly 20,000 cpm). Bound radioactivity collected from alkaline-lysed cells was quantified in a γ-spectrometer for the generation of competitive displacement curves in nonlinear regression analyses performed with Prism 3.02 (GraphPad Software, San Diego, CA). LIGAND software (25) was used to calculate dissociation constants (K_i values) for those receptors at which 1 μM unlabeled secretin displaced at least 70% of the bound radioligand.

Receptor Activity (cAMP) Assays: Receptor-expressing cells in 24-well plates also were tested for their ability to stimulate the production of cyclic AMP (cAMP) signaling molecules in response to agonist treatment (24). Briefly, intact PBS-washed cells were exposed to increasing amounts of secretin (from 0 to 1 μM) diluted in KRH containing 0.2% (w/v) bovine serum albumin, 0.01% (w/v) soybean trypsin inhibitor, 0.1% (w/v) bacitracin, and 1 mM 3-isobutyl-1-methylxanthine for 30 min at 37 °C. The cells then were acid-lysed and neutralized as described (24). The resulting supernatants were applied to radioactivity- (Diagnostic Products Corp., Los Angeles, CA) or fluorescence-based (Perkin Elmer, Wellesley, MA) competition binding assays according to the manufacturer's instructions (the former were discontinued during the course of this study). Bound ^{3}H-cAMP was recorded with a liquid scintillation counter; time-resolved FRET in LANCE assays was measured with an EnVision 2103 multilabel plate reader (Perkin Elmer). In both cases, counts were compared to standard curves for quantification of cAMP production and analysis of saturable displacements with Prism software. Second messengers produced by the first and second loop receptor variants represented less than 10% of the maximal response elicited by wild type receptors.

Spectral Microscopy: Spectral information was collected microscopically from live COS or CHO cells grown on 42-mm coverslips (Zeiss) in 6-cm Petri dishes. Transiently transfected COS cells were observed at steady state at 37 °C after mounting coverslips in an open cultivation POC-R cell chamber (Zeiss), and then washing and incubating in warm KRH containing bovine serum albumin and soybean trypsin inhibitor. Above-ambient temperatures were maintained with an aluminum Heating Insert P stage adaptor and Tempcontrol 37-2 digital temperature regulator (Zeiss). Stably transfected CHO cells were observed similarly by mounting coverslips in a pre-chilled POC-R chamber and rinsing cells with chilled KRH. Below-ambient temperatures for ligand incubations were created conductively by cooling the cell chamber with dry ice that was placed upon a pre-chilled stainless steel plate on top of the inactivated heatable stage adaptor. A temperature probe (Fluke, Everett, WA) fed through one of the perfusion ports in the stage adaptor was placed directly into the overlying KRH solution for real-time acquisitions of sample temperature. Cold-acclimated cells were imaged as described below, and then were treated for 30 min at 2 to 5 °C with secretin or PG97-269 ligands that were added directly to the overlying solution from appropriate 10-fold dilutions in KRH.

Spectral microscopy was performed with a Zeiss Axiovert 200M epifluorescence microscope that was equipped with an acousto-optic tunable filter (AOTF) imaging device custom-made by Chromodynamics, Inc. (Lakewood, NJ) (26). Samples were excited with 75-watt Xenon arc lamp (Zeiss) white light illumination that in the reflected light path was passed through a highly transmissive bandpass 400/45 nm excitation filter (Chroma Technology Corp, Rockingham, VT). Though not optimal for CFP excitation, this filter was combined in a standard epifluorescence filter cube with 440 nm beamsplitter and longpass 450 nm emission filters (Chroma) for the

collection of spectral information that included both CFP and YFP emissions. Signals greater than 450 nm were sent as a whole to the AOTF imaging device, which functioned as a dynamically-tuned, incremental bandpass filter for secondary modification of fluorescence emissions. A Photometrics (Tuscon, AZ) Cascade 128+ cooled CCD camera placed downstream of the AOTF imaging system was programmed to capture images in 5-nm increments from 460 to 600 nm without dynamic contrast adjustment. At these wavelengths, the AOTF device was capable of outputting very narrow bandwidths that increased evenly with the selected wavelength from roughly 1.5 to 3 nm, although this limited the overall throughput of the system to about 30% (including polarization losses) (26). This limitation was overcome in part by the multiplication gain capabilities of the Cascade camera. Digital 16-bit images were collected as 128 x 128 pixel frames with the camera operated in single frame mode; exposure times ranged from 25 to 500 ms (no binning) at gain settings of 3024 to 4095 with 2- to 12-fold averaging. AOTF manipulations and image acquisitions were automated with QED InVivo 2.2.0 software (Media Cybernetics, Silver Spring, MD) that had been modified by the manufacturer to include modules for AOTF control. In CHO cell experiments, this software also was used in conjunction with an MCU 28 motorized stage control unit (Zeiss) to mark multiple points of interest on the same coverslip and thus allow for the collection of spectral data from the same cells before and after ligand treatments. Based upon these conditions, each spectral data set consisted of a λ-stack of 29 separate TIFF images that when combined in series provided wavelength-specific intensity information for every pixel element of the micrograph.

FRET Calculations: FRET signals were derived from intensity-based spectral information according to (27) by first selecting an appropriate region(s) of interest (ROI) from a representative cell(s) in each data set. Whole-cell ROIs for COS cells were selected in MetaMorph 6.3 (Molecular Devices, Sunnyvale, CA) by creating boundaries around threshholded fluorescence emissions; plasma membrane ROIs for CHO cells were selected in QED InVivo as 5 x 5 pixel squares that were positioned at the cell periphery over only those areas of the membrane that appeared to possess authentic CFP and/or YFP fluorescence. It is important to note that plasma membrane ROIs were selected from the same cells in each image series before and after ligand incubations so that in these experiments comparisons could be drawn on a cell-by-cell basis. Average fluorescence intensities within each ROI, including a separate non-cellular ROI that represented non-specific (background) levels, then were exported to an Excel spreadsheet for every image in the spectral data set. Because each image corresponded to a specific emission wavelength, these background-corrected intensities either were normalized for the creation of spectral plots, or were integrated over defined bandwidths for the calculation of FRET ratios as follows: $[Em_{520\text{-}590}–(Em_{460\text{-}500}*Cf)]/Em_{460\text{-}500}$. The correction factor $Cf = Em_{520\text{-}590}/Em_{460\text{-}500}$ defined the proportion of the acceptor signal that was attributable to donor bleed-through, and was calculated separately for each experiment from spectral data sets of cells expressing the appropriate chameleon control that lacked the YFP acceptor. Donor-only controls in ligand experiments were treated and imaged identically to their corresponding chameleon samples for the calculation of separate, treatment-specific correction factors. Note that Cf is analogous to the donor bleed-through coefficient for sensitized emission calculations; acceptor bleed-through due to direct excitation of YFP with the 400/45 nm excitation filter was negligible (≤1% of maximal YFP emission). Spectral plots, bar graphs, and p values (unpaired student's t test) were generated in Prism 3.02.

RESULTS

Construction, Expression, and Subcellular Localization of Secretin Receptor Chameleons: Primary amino acid sequences of three secretin and seven closely-related vasoactive intestinal polypeptide receptors were aligned with the CLUSTALW algorithm to locate candidate sites within secretin receptor's predicted intracellular loop domains that may tolerate the insertion of a CFP reporter. Figure 1 shows these alignments and the positions that were chosen based upon the following criteria: a) the relative conservations of specific loop residues, b) the need to avoid the less well-defined boundaries between the predicted

loop and TM domains, and c) the demonstration of a successful insertion point in another receptor. All but one of the first loop residues were fully conserved, and thus forced attempted insertions into the middle two positions of the loop. The residues predicted to comprise the second loop were less well conserved than those of the shorter first loop, but only two of these amino acids provided favorable insertion points near the middle of the loop. The third and longest loop exhibited the most variability; here, the insertion site was chosen to match that utilized in the construction of a chameleon variant of the parathyroid hormone receptor (20). CFP insertions into each of these sites within carboxyl terminally-tagged SecR-YFP yielded a series of dual fluorescent reporter protein-tagged "chameleons" for intramolecular FRET analyses of receptor structure and/or activation (Fig. 1). Analogous insertions within an untagged, wild type SecR yielded the appropriate donor-only controls.

Each of the new chameleon receptor constructs was expressed individually in COS cells for microscopic assessments of subcellular localization. Panel *A* in Figure 2 shows a single optical section of a representative cell that possessed intracellular and plasma membrane fluorescence attributable to transiently expressed SecR-YFP within biosynthetic and cell surface compartments. Similar localization patterns were observed via YFP fluorescence for all three second and third loop chameleon receptors, although larger proportions of the total fluorescence signal appeared to originate from receptors in the endoplasmic reticulum and Golgi. The two first loop chameleon receptors were completely retained within these organelles, as well as within endoplasmic reticulum-associated aggregates at the cell periphery, and were not detected in the plasma membrane. Summarized in Table 1, these data confirm that the addition of YFP to the carboxyl terminus of SecR had no apparent effect on plasma membrane localization, and that receptors having CFP insertions in the second and third, but not the first, intracellular loops retained their ability to sort to the cell surface.

Functional Characterization of Chameleon Receptor Ligand Binding and Signaling: The chameleon receptor constructs capable of providing the most relevant structure-activity information would be those that exhibit binding and signaling characteristics similar to wild type receptors. The intact cell binding assay results shown in Figure 3 indicate that both the second and third loop variants satisfied this metric for ligand binding. Specifically, all four receptors that possessed a CFP reporter in either of two positions within the second intracellular loop bound secretin saturably and with high affinity. The K_i values listed in Table 1 show that their affinities were comparable to the nanomolar affinities typical of wild type secretin receptor, although the second loop variants bound only one-fourth the level of radiolabeled secretin that was bound by wild type receptors. Similar results were observed for the third loop variants, with these two receptors binding with nanomolar affinities three-fourths of the level of secretin that was bound by wild type (Table 1). None of the first loop variants exhibited saturable binding in intact COS cells, even at micromolar concentrations of ligand, consistent with the absence of these receptors within the plasma membrane. Cumulatively, these data suggest that secretin receptor's second and third intracellular loops tolerate reporter protein insertions and fold correctly for the maintenance of ligand binding function.

Figure 4 shows in graphical form the results of biological activity analyses. Unlike fully-functional wild type and carboxyl terminal YFP-tagged receptors, chameleon variants having a CFP moiety within the first intracellular loop were incapable of generating cAMP upon treatment of intact cells with stimulatory concentrations of secretin. As shown in Table 1, these receptors produced cAMP levels that were at or below the background levels (≤1 pmol) recorded in the absence of agonist. Receptors with second loop CFP insertions also were unable to elicit a secretin-stimulated cAMP response, despite their presence on the cell surface for ligand binding that was comparable to wild type receptors. Conversely, both third loop variants stimulated reproducible levels of cAMP at better than half the maximal response exhibited by wild type receptors. More specifically, the addition of a carboxyl-terminal YFP to either untagged or third loop CFP receptors allowed at least three-fourths the maximal output of wild type receptors. The

insertion of CFP within the third intracellular loop allowed for two-thirds maximal signaling and secretin efficacy to within two orders of magnitude as compared to wild type (Table 1). Together with the sorting and binding analyses, these results demonstrate that the first, second, and third loop variants provide non-functional, partially functional, and fully functional examples, respectively, of single and dual-tagged secretin receptors for structure activity studies.

Spectral Microscopic Analyses of Chameleon Receptor FRET: Each of the fluorescently-tagged chameleon receptors developed for the present study was evaluated microscopically for its ability to exhibit resonance energy transfer upon excitation of the donor fluorophore. It was predicted that differences in FRET among the loop receptor variants would reveal structural information about the relative positions of secretin receptor's intracellular loops and carboxyl terminal tail. A single representative was chosen for the first and second loop variants, namely the SecR(CFP^510)-YFP and SecR(CFP^732)-YFP receptors, because the alternate insertion points within these loops resulted in receptors that were functionally indistinguishable.

FRET signals were determined from single cells by a spectral imaging method that included the use of an acousto-optic tunable filter for the collection of a series of images at incremental emission wavelengths. As described in the Experimental Procedures, this method required the use of a blue-shifted filter for CFP excitation that limited bleed-through due to direct excitation of the acceptor to ≤1% of the signal recorded at YFP's excitation maximum. Photobleaching also was negligible because of the rapid response time of the acoustically-tuned emission filter; each image was acquired at millisecond exposure times that allowed for total capture durations of 10-45 seconds for an entire image series. Figure 5*A* shows a representative series collected in 5-nm increments from 460-600 nm upon excitation at 400 nm of a single living COS cell transiently expressing the third loop chameleon receptor. As a whole, the fluorescence intensities of the images varied with acquisition wavelength according to the expected emission signatures of the incorporated CFP donor and YFP acceptor. Specifically, virtually no fluorescence was detected at the ends of the spectral region scanned from 460-480 nm and from 580-600 nm, whereas peak intensities occurring at 520-550 nm fell within a range of prominent signals that were detected from 480-580 nm. Analogous data were acquired from cells expressing the first and second loop chameleon receptors, as well from cells expressing the appropriate control receptors tagged singly with only the donor or acceptor fluorophore. Though image quality was traded in these experiments for camera sensitivity, all receptors were observed routinely within the same intracellular and plasma membrane compartments that were seen in the confocal analyses shown in Figure 2.

Wavelength-registered intensity information included in the images in Figure 5*A* was extracted from appropriate pixels of interest for the subsequent correction and quantification of spectral relationships, including FRET. In these experiments, "appropriate" pixels were those within custom-shaped regions of interest defined by threshholding total cellular fluorescence that included both intracellular and plasma membrane organelles. Figure 5*B* shows the spectral profiles of the average pixel intensities within these regions, as well as within similar regions from image sets of representative controls, after background subtraction and normalization. Cells expressing the CFP-only third loop control receptor gave two peaks of fluorescence at 480 nm and 505 nm, whereas those expressing the YFP-only carboxyl terminal control receptor gave a single peak of fluorescence at 525 nm. The broad emission spectrum of cells expressing the dual-tagged third loop chameleon included emissions that coincided with the sharper fluorescence peaks of the corresponding donor- and acceptor-only controls. The normalized intensities of the CFP portion of this signal roughly were one-fifth of the intensities of the YFP portion, suggesting that the former was suppressed by donor quenching due to FRET. Similar spectral profiles were observed for first and second loop variant receptors, and all fluorescence signals were confirmed for each receptor independently in spectrofluorometry assays that employed suspensions of live, receptor-expressing COS cells (data not shown).

Intensity data from chameleon receptors and their corresponding donor-only controls were integrated across CFP- and YFP-specific wavelengths to remove the large proportion of donor signal that was observed in the acceptor portion of the spectrum (Fig. 5*B*). Figure 5*C* shows the resulting bleed-through-corrected signals after normalizing against the total donor signal to minimize expression level variations. All three chameleon receptors exhibited robust FRET signals that varied significantly with the position of the CFP donor. Specifically, the FRET ratio derived from the first loop chameleon was over twice that observed for the second loop chameleon, and the latter was just over half the FRET ratio calculated for the third loop chameleon. Because the efficiency of energy transfer depends largely on the distance between the donor and acceptor fluorophores, these FRET data may provide an indication of the relative position of each loop with respect to the carboxyl terminus. Thus, it is likely that at steady state the first and second intracellular loops of intact secretin receptor are situated closest and furthest from the carboxyl terminal tail, respectively, with the third loop of the receptor intermediate in its distance from the tail. It should be noted that these predictions are stated in relative, rather than absolute, terms because the fluorescence lifetime measurements needed for the determination of FRET efficiencies could not be acquired under the same conditions with the spectral microscope.

Spectral Microscopic Analyses of Stably-Expressed, Plasma Membrane-Localized Third Loop Chameleon Receptors in Ligand-Treated Cells: The FRET signal observed between the third intracellular loop and carboxyl terminus of the fully-functional third loop chameleon provided an opportunity to study the predicted conformational changes of these domains upon ligand-mediated receptor activation. Stable transfections were employed to minimize experimental differences associated with transient gene (over)expression. In the CHO cell system, these receptors bound secretin saturably (K_i, 1.89 ± 0.15 nM) and with an affinity comparable to that recorded from a well-characterized cell line that stably expresses wild type human SecR (K_i, 0.71 ± 0.06 nM). Similar results were obtained for a separate CHO cell line made to express the SecR(CFP^993) third loop control receptor (K_i, 1.02 ± 0.20 nM).

Figure 6*A* shows two micrographs from a spectral data set that depict fluorescence emissions at 460 and 525 nm from a representative CHO cell stably expressing the third loop chameleon receptor. Like the COS cell example in Figure 5*A*, the emission intensity varied with wavelength according to the predicted outputs of the CFP and YFP reporters. Specifically, the prominent signal at 525 nm included plasma membrane labeling that largely was absent at 460 nm but was consistent with the localization of this receptor in COS cells (Fig. 2*F*). These and similar data acquired from the same cells after 30-min treatments with secretin receptor ligands were used to generate the emission spectra shown in Figure 6*B*, which represent intensity information from regions of interest that included only fluorescence attributable to receptors localized within the plasma membrane. The spectra show that stimulatory concentrations of secretin (0.1 μM) caused a marked decrease in plasma membrane YFP fluorescence at 525 nm relative to the CFP signal at 480 nm. These conditions did not change the broad CFP emission profiles of donor-only control receptors (Fig. 6*B*). Shown in Figure 6*C*, this difference corresponded to a two-thirds decrease in FRET that was not observed in cells that were treated with the secretin receptor antagonist PG97-269. All treatments were performed at or near 4 °C to minimize the downstream processes of internalization and desensitization over and subsequent to the 30-min incubation period. The FRET decrease was not due to cell-to-cell variations in expression level or overall photobleaching during image acquisition, because the data were normalized on a cell-by-cell basis against the steady state signals achieved before ligand applications. In addition, bleed-through corrections were performed separately using coefficients calculated both before and after treatments to ensure that changes in the FRET signal were not due to donor quenching that was independent of the FRET response. Finally, it is unlikely that the observed FRET signals were derived from intermolecular energy transfer between stably oligomerized receptors, because secretin has been shown to have no effect on intermolecular BRET signals recorded from

tagged secretin receptors in agonist-stimulated cells (28). The observation that this significant decrease in FRET was observed only upon agonist treatment suggests that it reflects a translational and/or rotational response of the incorporated fluorophores as a measurable characteristic of secretin binding.

DISCUSSION

Resonance energy transfer techniques have become powerful and popular approaches for elucidating various aspects of GPCR structure (29,30). However, it is uncommon for these approaches to incorporate into the same receptor molecule two fluorescent reporters for the detection of intramolecular energy transfer events. Applied to soluble nuclear receptors, this approach has been employed successfully in the demonstration of a hormone-induced conformational change in androgen receptors that had been appended at their amino and carboxyl termini with CFP and YFP reporters (31). However, this method has not been reported often for complex membrane receptors, most likely because the inclusion of multiple bulky fluorophores leads to defects in receptor sorting and/or function. This certainly was the case in the present study (see below), as it was in the only other report of intramolecular FRET in GPCRs, a closely-related study that determined the kinetics of conformational changes within CFP/YFP chameleons of the α_{2A}-adrenergic and parathyroid hormone receptors (20). In that study, third loop chameleons were the only ones employed because all others exhibited functional defects and were determined to be unfit for kinetic analyses. A recent report attempted to address these concerns by targeting a much smaller biarsenical fluorescein acceptor to a tetracysteine motif that had been incorporated into a CFP-tagged receptor (32).

Although the chameleon secretin receptors generated for this study were designed primarily for intramolecular FRET applications, their characterizations provided valuable information on the functional importance of the receptor's intracellular loop and carboxyl-terminal domains. For example, appending secretin receptor with a carboxyl-terminal YFP had no measurable effect on the plasma membrane sorting, ligand binding, or cAMP signaling capabilities of the modified receptor. Located at the end of what is presumed to be a flexible tail region, this position has been shown to tolerate various reporter proteins with little effect on function (28), even when truncated to remove several known phosphorylation sites for receptor regulation (22,33). Conversely, insertions of a CFP moiety into the first intracellular loop resulted in non-sorting receptors that largely remained trapped within biosynthetic organelles. This sorting defect effectively limited their exposure to applied ligand and thus prevented secretin binding and biological activity. The first loop was an interesting candidate for tag insertion in that modification of a nearby histidine residue at the cytosolic end of the second TM helix created a fully-functional receptor with moderate constitutive activity (34). Placement of the CFP tag at either of two positions within the small, highly-conserved loop yielded no significant differences in sorting, and neither position afforded the constitutive activity observed with the single histidine substitution. Each of the first loop chameleon variants did, however, exhibit CFP, YFP, and FRET fluorescence signals that indicated at least some level of fusion protein maturation. Though the presence of fluorescent aggregates in some transfected cells suggested likely disruption in the folding and/or maturation of these receptors, it seems clear from the data presented here that the first intracellular loop may provide a turn region that is critical for the proper insertion of the first and second TM helices into the membrane or for the proper spacing and spatial relationships between these helices.

CFP insertions within the second intracellular loop generated a unique set of receptor variants that were functionally distinct from the non-sorting first loop mutants. The former were found localized in the plasma membrane and were competent for secretin binding with wild type affinities. Of note, the abilities of these second loop variants to bind agonist did not correlate with their abilities to stimulate cAMP production, suggesting that agonist binding may have been unable to elicit the conformational changes needed for receptor activation. Similar conclusions were drawn from a parathyroid hormone receptor mutant in which an endogenous histidine at the cytosolic end of helix three supported the formation of zinc-binding

bridges to helix six that inhibited downstream signaling but not ligand binding (4). The second intracellular loop is an important determinant of the efficiency with which a receptor activates its cognate G protein(s) (35), although this characteristic has not been verified to great detail for Family B receptors. Nonetheless, it is likely that the steric hindrance exerted by the second loop CFP prevented secretin receptor from interacting efficiently with its downstream effectors. It is our conclusion that this loop in secretin receptor is important for G protein coupling, and according to the results presented here provides an interesting and unusual means for uncoupling ligand binding from receptor activation.

Of all the receptor variants prepared for the present study, the third loop chameleon receptors retained functions that were most like wild type. Specifically, these receptors bound secretin saturably and with high affinity at the plasma membrane, and this binding was shown to elicit cAMP production as evidence of biological activity. Half-maximal cAMP responses required an effective concentration of secretin (EC_{50}) that was approximately 100 times greater than that recorded for wild type or carboxyl terminally-tagged receptors. This result is consistent with the biological activities of third loop chameleons of the α_{2A}-adrenergic and parathyroid hormone receptors (20), indicating clearly that third loop CFP insertions most likely obstruct, but do not eliminate, coupling to G protein subunits. Thus, the larger third intracellular loop seems to be a flexible linker that is more tolerant of modifications than other intracellular regions, making this loop the best candidate for insertions of bulky fluorescent reporter proteins.

FRET signals were recorded consistently from each of the five chameleon secretin receptors, and each chameleon type yielded a unique FRET signal that could be correlated with the different intracellular loop positions of the CFP donor. The data suggest that the carboxyl terminus is positioned closest to the first loop and furthest from the second loop. One arrangement that is consistent with these relative positions would be for the carboxyl terminus to reside on the side of the inactivated receptor that is opposite the second intracellular loop. This interpretation must be taken with caution, however, due to the possibility for misfolding in the first loop variants. FRET signals were observed on both a standard spectrofluorometer and our spectral imaging workstation, but the latter provided several advantages for imaging FRET with increased sensitivity at the single cell level. In particular, spectral imaging circumvented the limitations of standard epifluorescence microscopes that utilize bandpass filters with fixed cutoff parameters, thus allowing for better spectral separation of fluorescence signatures that could be registered to every pixel in the image (27,36). In practice, these features allowed for more accurate removal of background autofluorescence and donor bleed-through, the latter of which is a significant factor for the CFP/YFP FRET pair (22,28). Applying an AOTF in this manner is to our knowledge unreported, because all other applications of these filters for detection of exogenous fluorescence thus far have set the AOTF at static wavelengths (26,37) or have unmixed multiple signatures that did not include FRET (38). This is significant since the microsecond switching capabilities of the AOTF instrument (26) make it theoretically possible to detect rapid changes in distances.

The spectral imaging approach also provided a highly-sensitive means for detecting agonist-induced changes in the FRET signal. In cells stably expressing fully-functional third loop chameleons, an observed decrease in FRET suggested that the relative positions of the carboxyl terminus and third loop of secretin receptor moved away from each other upon agonist, but not antagonist, binding. A similar conclusion was derived from the decreased FRET observed with α_{2A}-adrenergic and parathyroid hormone receptor chameleons (20), where a subsequent study also observed differential effects of specific agonist and antagonist ligands at the former (39). In those studies, it was argued for α_{2A}-adrenergic receptors that the possible movement of the third loop away from the carboxyl terminus correlated with predicted agonist-induced changes in the TM helices of Family A GPCRs, and that a common mechanism could exist for Family A and B receptors. Establishing this clearly will require substantial additional evidence.

ACKNOWLEDGMENTS

We appreciate the excellent technical assistance of Renee Happs, Laura Bruins, and Delia Pinon. We also thank Elliot Wachman (Chromodynamics, Inc., Lakewood, NJ) and Ciprian Almonte (Media Cybernetics, Silver Spring, MD) for helpful discussions and suggestions regarding use and application of the AOTF system and QED InVivo software.

REFERENCES

1. Karnik, S. S., Gogonea, C., Patil, S., Saad, Y., and Takezako, T. (2003) *Trends Endocrinol Metab* **14**, 431-437
2. Bissantz, C. (2003) *J Recept Signal Transduct Res* **23**, 123-153
3. Okada, T., and Palczewski, K. (2001) *Curr Opin Struct Biol* **11**, 420-426
4. Sheikh, S. P., Vilardarga, J. P., Baranski, T. J., Lichtarge, O., Iiri, T., Meng, E. C., Nissenson, R. A., and Bourne, H. R. (1999) *J Biol Chem* **274**, 17033-17041
5. Donnelly, D. (1997) *FEBS Lett* **409**, 431-436
6. Beinborn, M. (2006) *Mol Pharmacol* **70**, 1-4
7. Dong, M., and Miller, L. J. (2002) *Receptors Channels* **8**, 189-200
8. Dong, M., Wang, Y., Hadac, E. M., Pinon, D. I., Holicky, E., and Miller, L. J. (1999) *J Biol Chem* **274**, 19161-19167
9. Dong, M., Wang, Y., Pinon, D. I., Hadac, E. M., and Miller, L. J. (1999) *J Biol Chem* **274**, 903-909
10. Dong, M., Asmann, Y. W., Zang, M., Pinon, D. I., and Miller, L. J. (2000) *J Biol Chem* **275**, 26032-26039
11. Dong, M., Zang, M., Pinon, D. I., Li, Z., Lybrand, T. P., and Miller, L. J. (2002) *Mol Endocrinol* **16**, 2490-2501
12. Zang, M., Dong, M., Pinon, D. I., Ding, X. Q., Hadac, E. M., Li, Z., Lybrand, T. P., and Miller, L. J. (2003) *Mol Pharmacol* **63**, 993-1001
13. Dong, M., Li, Z., Zang, M., Pinon, D. I., Lybrand, T. P., and Miller, L. J. (2003) *J Biol Chem* **278**, 48300-48312
14. Dong, M., Li, Z., Pinon, D. I., Lybrand, T. P., and Miller, L. J. (2004) *J Biol Chem* **279**, 2894-2903
15. Dong, M., Pinon, D. I., and Miller, L. J. (2005) *Mol Endocrinol* **19**, 1821-1836
16. Dong, M., Pinon, D. I., Asmann, Y. W., and Miller, L. J. (2006) *Mol Pharmacol* **70**, 206-213
17. Dong, M., Hosohata, K., Pinon, D. I., Muthukumaraswamy, N., and Miller, L. J. (2006) *Mol Endocrinol* **20**, 1688-1698
18. Harikumar, K. G., Hosohata, K., Pinon, D. I., and Miller, L. J. (2006) *J Biol Chem* **281**, 2543-2550
19. Castro, M., Nikolaev, V. O., Palm, D., Lohse, M. J., and Vilardaga, J. P. (2005) *Proc Natl Acad Sci U S A* **102**, 16084-16089
20. Vilardaga, J. P., Bunemann, M., Krasel, C., Castro, M., and Lohse, M. J. (2003) *Nat Biotechnol* **21**, 807-812
21. Powers, S. P., Pinon, D. I., and Miller, L. J. (1988) *Int J Pept Protein Res* **31**, 429-434
22. Lisenbee, C. S., and Miller, L. J. (2006) *Biochemistry* **45**, 8216-8226
23. Cheng, Z. J., and Miller, L. J. (2001) *J Biol Chem* **276**, 48040-48047
24. Lisenbee, C. S., Dong, M., and Miller, L. J. (2005) *J Biol Chem* **280**, 12330-12338
25. Munson, P. J., and Rodbard, D. (1980) *Anal Biochem* **107**, 220-239
26. Wachman, E. S., Niu, W., and Farkas, D. L. (1997) *Biophys J* **73**, 1215-1222
27. Ecker, R. C., de Martin, R., Steiner, G. E., and Schmid, J. A. (2004) *Cytometry A* **59**, 172-181
28. Harikumar, K. G., Morfis, M. M., Lisenbee, C. S., Sexton, P. M., and Miller, L. J. (2006) *Mol Pharmacol* **69**, 363-373

29. Eidne, K. A., Kroeger, K. M., and Hanyaloglu, A. C. (2002) *Trends Endocrinol Metab* **13**, 415-421
30. Hebert, T. E., Gales, C., and Rebois, R. V. (2006) *Cell Biochem Biophys* **45**, 85-109
31. Schaufele, F., Carbonell, X., Guerbadot, M., Borngraeber, S., Chapman, M. S., Ma, A. A., Miner, J. N., and Diamond, M. I. (2005) *Proc Natl Acad Sci U S A* **102**, 9802-9807
32. Hoffmann, C., Gaietta, G., Bunemann, M., Adams, S. R., Oberdorff-Maass, S., Behr, B., Vilardaga, J. P., Tsien, R. Y., Ellisman, M. H., and Lohse, M. J. (2005) *Nat Methods* **2**, 171-176
33. Ozcelebi, F., Holtmann, M. H., Rentsch, R. U., Rao, R., and Miller, L. J. (1995) *Mol Pharmacol* **48**, 818-824
34. Ganguli, S. C., Park, C. G., Holtmann, M. H., Hadac, E. M., Kenakin, T. P., and Miller, L. J. (1998) *J Pharmacol Exp Ther* **286**, 593-598
35. Gether, U. (2000) *Endocr Rev* **21**, 90-113
36. Zimmermann, T. (2005) *Adv Biochem Eng Biotechnol* **95**, 245-265
37. Wachman, E. S., Poage, R. E., Stiles, J. R., Farkas, D. L., and Meriney, S. D. (2004) *J Neurosci* **24**, 2877-2885
38. Farkas, D. L., and Becker, D. (2001) *Pigment Cell Res* **14**, 2-8
39. Lohse, M. J., Vilardaga, J. P., and Bunemann, M. (2003) *Life Sci* **74**, 397-404

FOOTNOTES

[1] This work was supported by grants from the National Institutes of Health (DK46577) and the Fiterman Foundation.

[2] The abbreviations used are: AOTF, acousto-optic tunable filter; CFP, cyan fluorescent protein; CHO, Chinese hamster ovary; DMEM, Dulbecco's modified Eagle's growth medium; FRET, fluorescence resonance energy transfer; GPCR, G protein-coupled receptor; SecR, secretin receptor; TM, transmembrane; YFP, yellow fluorescent protein.

FIGURE LEGENDS

FIGURE 1. **Structural representations of membrane-bound SecR and dual reporter-tagged SecR constructs.** The diagrams on the left compare to an unmodified wild type receptor (A) three groups of "chameleon" receptor constructs having CFP in the first (two positions) (B), second (two positions) (C) or third (one position) (D) intracellular loops and YFP at the carboxyl terminus. The predicted amino acid sequences on the right correspond to the intracellular loops (bold) of human SecR and their degrees of similarity to other secretin and closely-related vasoactive intestinal polypeptide receptors (*, fully conserved residue; :, conservation of strong groups; ., conservation of weak groups; <space>, no consensus). Numbers refer to the nucleotide positions after which the open reading frame of the CFP reporter was inserted (arrowheads). Donor- and acceptor-only control constructs lacked the appropriate YFP or CFP moieties, respectively (not shown). Diagrams modified from (20).

FIGURE 2. **Fluorescence localizations of chameleon secretin receptors.** Representative confocal micrographs (single optical sections) of formaldehyde-fixed COS cells exhibiting plasma membrane and/or intracellular fluorescence attributable to direct excitation of the YFP reporter of chameleon receptors. Unlike the YFP-tagged wild type receptor (A), the first loop chameleons, SecR(CFP^510)-YFP (B) and SecR(CFP^513)-YFP (C), did not sort to the plasma membrane and instead remained trapped within the endoplasmic reticulum and reticulum-associated aggregates. All other receptor variants sorted normally to the plasma membrane, including the second loop chameleons, SecR(CFP^732)-YFP (D) and SecR(CFP^735)-YFP (E), and the third loop variant, SecR(CFP^993)-YFP (F). Bar in (A) = 25 μm.

FIGURE 3. **Ligand binding capabilities of donor-only and chameleon secretin receptors.** Each panel demonstrates the abilities of increasing concentrations of natural secretin agonist to compete for the binding of a radioiodinated ^{125}I-[Tyr^{10}]secretin analog to intact COS cells expressing the first (A), second (B), or third (C) loop receptor variants indicated. Data represent saturable binding as percentages of the maximal responses achieved in the absence of competitor (means ± S.E.M. from three or more experiments performed in duplicate).

FIGURE 4. **Biological activities of donor-only and chameleon secretin receptors.** Each panel shows the relative levels of intracellular cAMP produced upon stimulation with increasing concentrations of secretin of roughly 25,000 COS cells expressing the first (A), second (B), or third (C) loop receptor variants indicated (means ± S.E.M. of duplicate data points from three or more independent experiments).

FIGURE 5. **FRET analyses of representative first, second, and third loop chameleon secretin receptors.** (A) Fluorescence micrographs of a representative chameleon receptor-expressing COS cell excited with a CFP-specific bandpass filter. Fluorescence emissions were selected with an acousto-optic tunable filter and captured with a CCD camera set to collect images in 5-nm increments from 460 to 600 nm. The final panel shows the cellular and background regions of interest (ROI) from which wavelength-specific intensity data were derived. Bar = 50 μm. (B) Microscopically-derived fluorescence emission spectra of living COS cells expressing the receptor variants indicated. The spectra were generated by plotting as a function of the acquisition wavelength the background-subtracted, normalized fluorescence intensities of cellular ROIs similar to the example depicted in (A). Cells expressing CFP donor- (λ_{ex} = 400 nm) or YFP acceptor-only (λ_{ex} = 480 nm) control receptors exhibited peak emissions at 505 and 525/530 nm, respectively, whereas cells expressing chameleon receptors (λ_{ex} = 400 nm) displayed donor-suppressed FRET emissions that peaked at wavelengths corresponding to the YFP acceptor. (C) FRET signals of living COS cells expressing independently each of the three chameleon receptors indicated. The FRET signals represent the mean bleed-through-corrected YFP emissions from 4 to 6 cells in as many spectral data sets. *, $p < 0.05$; **, $p < 0.001$.

FIGURE 6. **FRET analyses of third loop chameleon secretin receptors expressed stably in CHO cells.** (A) Representative stack of wavelength-registered fluorescence micrographs showing SecR(CFP^993)-YFP receptors localized to the plasma membranes and biosynthetic organelles of living cells in culture. Acousto-optic tunable filter-selected emissions were collected from the same cells incubated at 4 °C before and after treatment with secretin agonist or PG97-269 antagonist. The two squares mark regions of interest (ROI) over non-cellular background and plasma membrane portions of the images from which intensities were calculated for generating emission spectra and FRET ratios. Bar = 5 μm. (B) Fluorescence emission spectra of living CHO cells expressing the indicated third loop donor-only control or chameleon receptors in the absence or presence of 0.1 μM secretin. The spectra represent average background-subtracted and normalized intensities within plasma membrane ROIs of cells excited at donor-specific wavelengths (λ_{ex} = 400 nm). (C) Plasma membrane-specific FRET responses of ligand-treated CHO cells. Sensitized FRET signals (bleed-through-corrected YFP emissions) derived from integrated fluorescence intensities within plasma membrane ROIs were normalized on a cell-by-cell basis against the untreated condition. The data are expressed as the mean normalized FRET signals from roughly 15 cells in at least five spectral data sets. **, $p < 0.001$; the values represented by the first and third bars were not significantly different from each other ($p>0.05$).

TABLE 1

Functional characteristics of chameleon secretin receptor mutants

Receptor constructs	Secretin binding		Biological activity		PM sorting[b]
	K_i (nM)	% WT[a]	Max (pmol)	EC_{50} (nM)	
SecR	4.6 ± 1.0	100.0 ± 0.0	39.6 ± 3.1	0.01 ± 0.001	
SecR-YFP	6.2 ± 2.4	104.4 ± 0.4	31.7 ± 0.9	0.02 ± 0.008	+++
SecR(CFP^510)	>1000	<5	<1	>1000	
SecR(CFP^510)-YFP	>1000	<5	<1	>1000	–
SecR(CFP^513)	>1000	<5	<1	>1000	
SecR(CFP^513)-YFP	>1000	<5	<1	>1000	–
SecR(CFP^732)	3.1 ± 0.7	25.7 ± 1.5	<1	>1000	
SecR(CFP^732)-YFP	1.4 ± 0.3	23.0 ± 2.8	<1	>1000	+
SecR(CFP^735)	3.1 ± 1.1	27.3 ± 1.7	<1	>1000	
SecR(CFP^735)-YFP	2.3 ± 0.7	21.2 ± 3.3	<1	>1000	+
SecR(CFP^993)	5.1 ± 1.7	78.3 ± 4.5	26.9 ± 1.7	0.7 ± 0.3	
SecR(CFP^993)-YFP	3.6 ± 1.6	74.0 ± 8.5	20.3 ± 0.8	1.2 ± 0.4	+

[a] Percent bound in absence of competitor with respect to untagged wild type receptors.

[b] Substantial (+++), partial (+), or no (–) plasma membrane (PM) sorting of YFP-tagged receptors visualized in COS cells via confocal fluorescence microscopy.

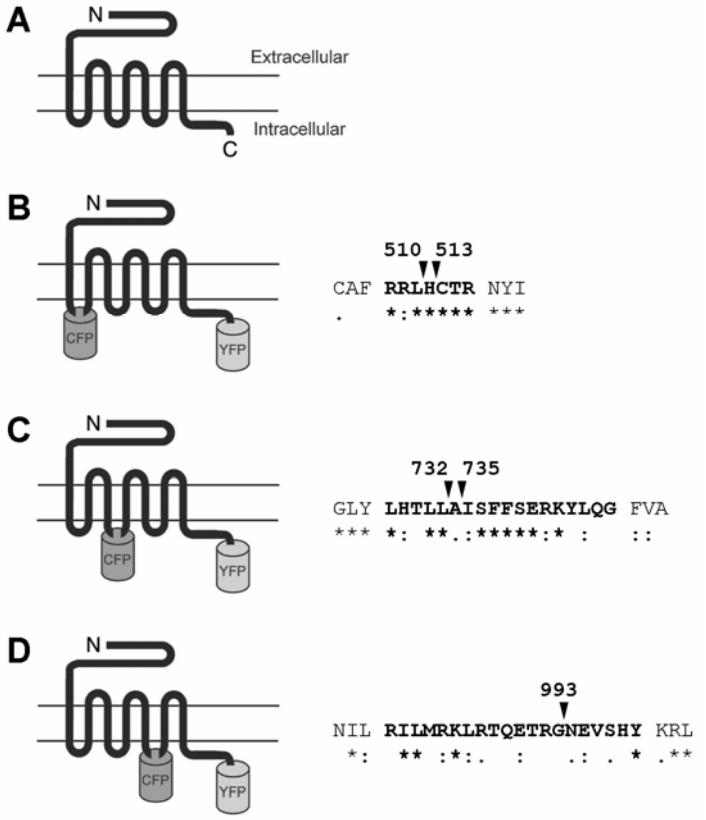

Figure 1. Lisenbee et al.

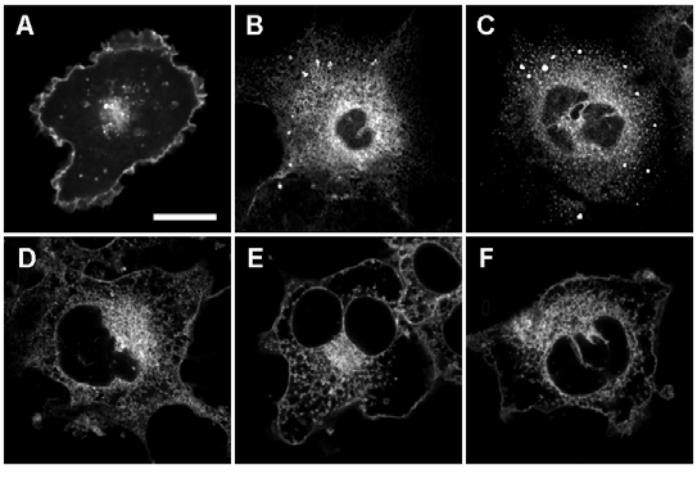

Figure 2. Lisenbee et al.

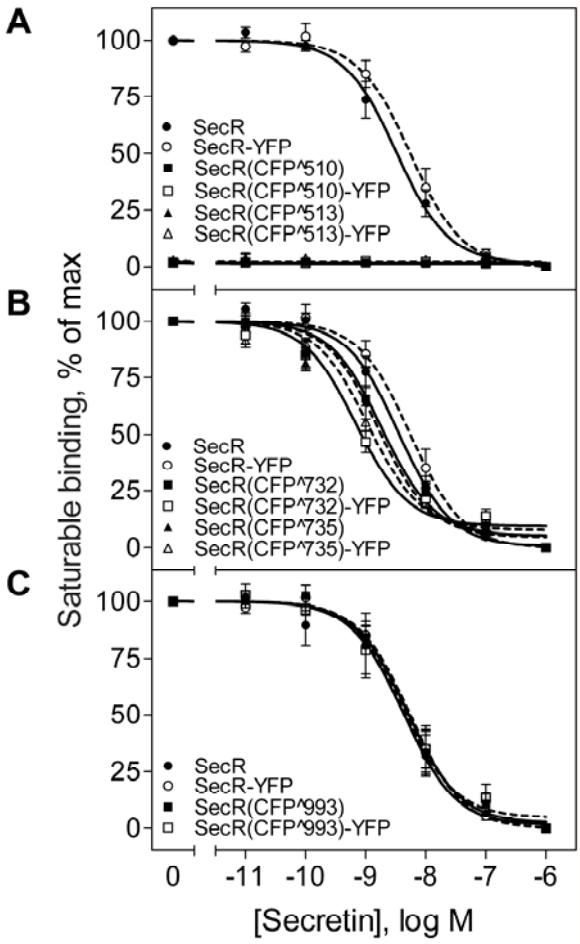

Figure 3. Lisenbee et al.

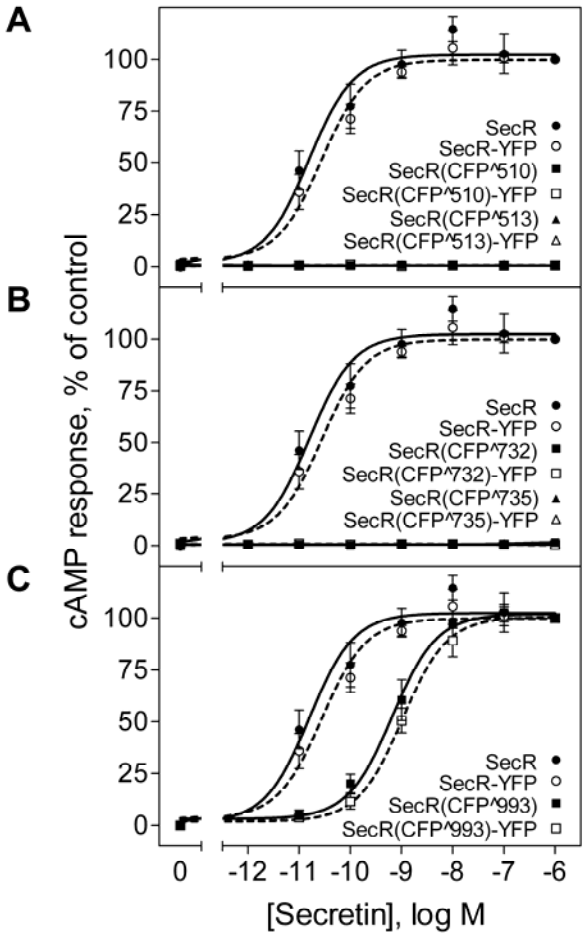

Figure 4. Lisenbee et al.

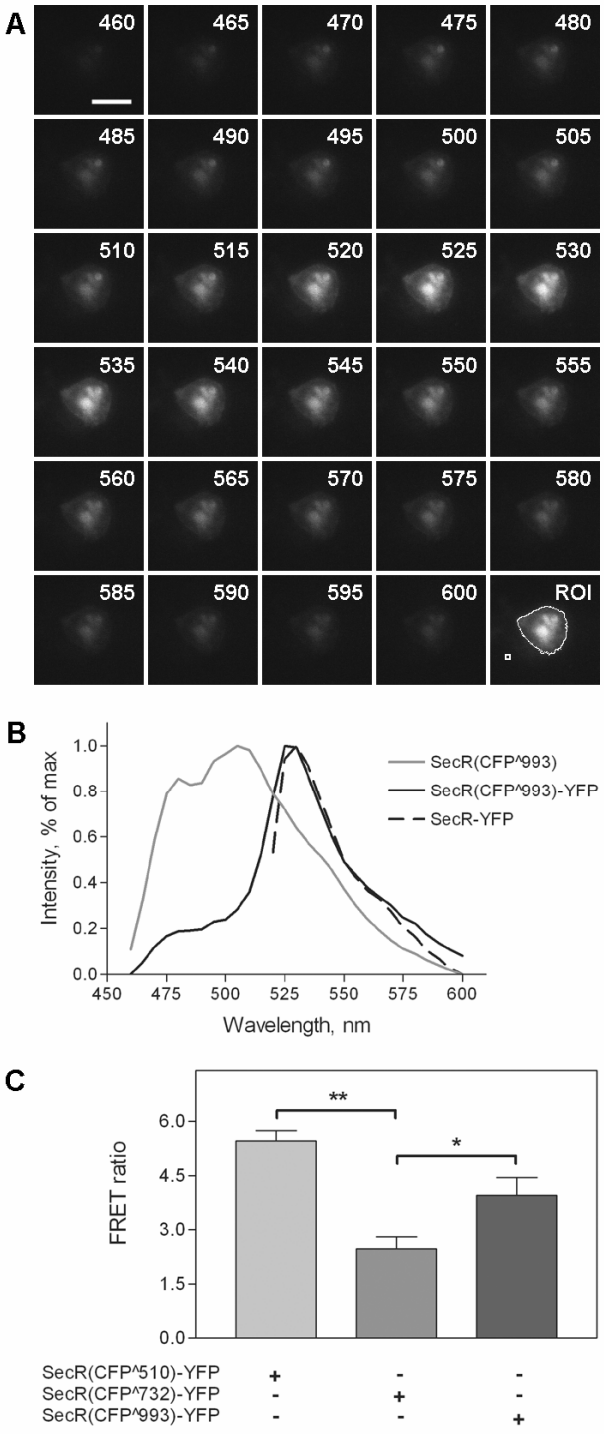

Figure 5. Lisenbee et al.

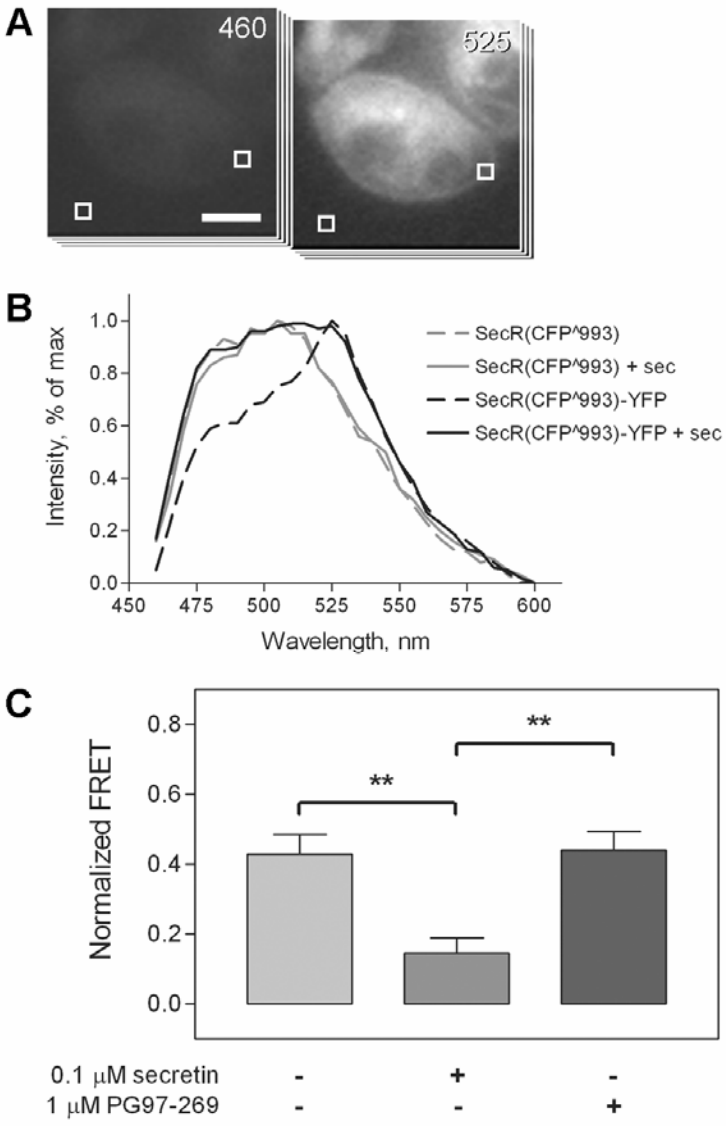

Figure 6. Lisenbee et al.